

Excellence in Chemistry Research

Announcing our new flagship journal

- Gold Open Access
- Publishing charges waived
- Preprints welcome
- Edited by active scientists



Meet the Editors of *ChemistryEurope*



Luisa De Cola

Università degli Studi
di Milano Statale, Italy



Ive Hermans

University of
Wisconsin-Madison, USA



Ken Tanaka

Tokyo Institute of
Technology, Japan

Quantum Yield of DNA Strand Breaks under Photoexcitation of a Molecular Ruby

Cui Wang^{+, [a, d]} Kenny Ebel^{+, [b]} Katja Heinze,^[c] Ute Resch-Genger,^{*, [a]} and Ilko Bald^{*, [b]}

Abstract: Photodynamic therapy (PDT) used for treating cancer relies on the generation of highly reactive oxygen species, for example, singlet oxygen $^1\text{O}_2$, by light-induced excitation of a photosensitizer (PS) in the presence of molecular oxygen, inducing DNA damage in close proximity of the PS. Although many precious metal complexes have been explored as PS for PDT and received clinical approval, only recently, the potential of photoactive complexes of non-noble metals as PS has been discovered. Using the DNA origami technology that can absolutely quantify DNA strand

break cross sections, we assessed the potential of the luminescent transition metal complex $[\text{Cr}(\text{ddpd})_2]^{3+}$ (ddpd = *N,N'*-dimethyl-*N,N'*-dipyridine-2-ylpyridine-2,6-diamine) to damage DNA in an air-saturated aqueous environment upon UV/Vis illumination. The quantum yield for strand breakage, that is, the ratio of DNA strand breaks to the number of absorbed photons, was determined to 1–4%, indicating efficient transformation of photons into DNA strand breaks by $[\text{Cr}(\text{ddpd})_2]^{3+}$.

Introduction

Photodynamic therapy (PDT) is a therapeutic modality that induces locally controlled cell death in cancerous tissues by light with the aid of a photosensitizer (PS). For example, some PS like Photofrin, that is approved by the Food and Drug Administration (FDA), is used for the clinical treatments of bladder cancer, lung cancer, and oesophageal cancer.^[1] Upon light absorption, the excited singlet state of the PS is populated, followed by subsequent intersystem crossing (ISC) to the long-lived triplet state. The triplet state can be then depopulated

radiatively yielding phosphorescence and non-radiatively by (Dexter-type) energy transfer to triplet molecular oxygen ($^3\text{O}_2$), leading to the formation of cytotoxic singlet oxygen ($^1\text{O}_2$, Type II).^[2,3] Depending on the excited state redox potential of the PS, electron transfer between the PS and the environment can occur, resulting in the formation of radical intermediates that can further generate reactive oxygen species (ROS) such as $\text{O}_2^{\bullet-}$ and OH^{\bullet} (Type I).^[2b,4] These reactions, yielding $^1\text{O}_2$ and/or other ROS, can subsequently induce highly localized necrotic and/or cell death of the targeted cancer cells or tissues.^[5]

An ideal PS should strongly absorb visible or near infrared (NIR) light, have a long excited state lifetime, and no dark cytotoxicity.^[6] To date, there exists a large toolbox of PSs including organic dyes,^[7] like the first-generation PS Photofrin derived from porphyrins,^[8] as well as phthalocyanine,^[9] indocyanine,^[10] and boron-dipyrromethene (BODIPY),^[11] pyridinium alkynylanthracene,^[12] diketopyrrolopyrrole (DPP),^[13] and aggregation-induced emission dyes.^[14] In addition, photoactive complexes made of precious metals, such as Au^{III} , Pt^{II} , Pd^{II} , Ir^{III} , Ru^{II} or Os^{II} have been used.^[15] Recently, also complexes of earth-abundant metals such as Cu^{I} , Fe^{II} or Fe^{III} , Cr^{III} , and Zn^{II} have been explored as PS.^[15d,16] These metal ions are mostly bio-essential, thus minimizing undesired dark toxicity caused by heavy metals such as Pt^{II} .^[17]

Until now, there are only few examples employing Cr^{III} complexes for PDT despite their interesting optical properties.^[18] For example, the molecular ruby $[\text{Cr}(\text{ddpd})_2]^{3+}$ (ddpd = *N,N'*-dimethyl-*N,N'*-dipyridine-2-ylpyridine-2,6-diamine) (Scheme 1a) shows a strong spin-flip emission in the near-infrared (NIR) range with record phosphorescence quantum yields (Φ_p) of up to 30% and millisecond lifetimes (τ) in deaerated solutions at room temperature.^[19] These developments meanwhile initiated applications of these Cr^{III} complexes in sensing,^[19a,20] photocatalysis,^[21] energy upconversion,^[22] and circularly polarized luminescence.^[23] In aerated water, the doublet excited


[a] Dr. C. Wang,⁺ Dr. U. Resch-Genger
Division Biophotonics
Federal Institute for Materials Research and Testing (BAM)
Richard-Willstaetter Strasse 11, 12489 Berlin (Germany)
E-mail: ute.resch@bam.de


[b] Dr. K. Ebel,⁺ Prof. Dr. I. Bald
Institute of Chemistry, Hybrid Nanostructures
University of Potsdam
Karl-Liebknecht-Str. 24–25, 14476 Potsdam (Germany)
E-mail: ilko.bald@uni-potsdam.de

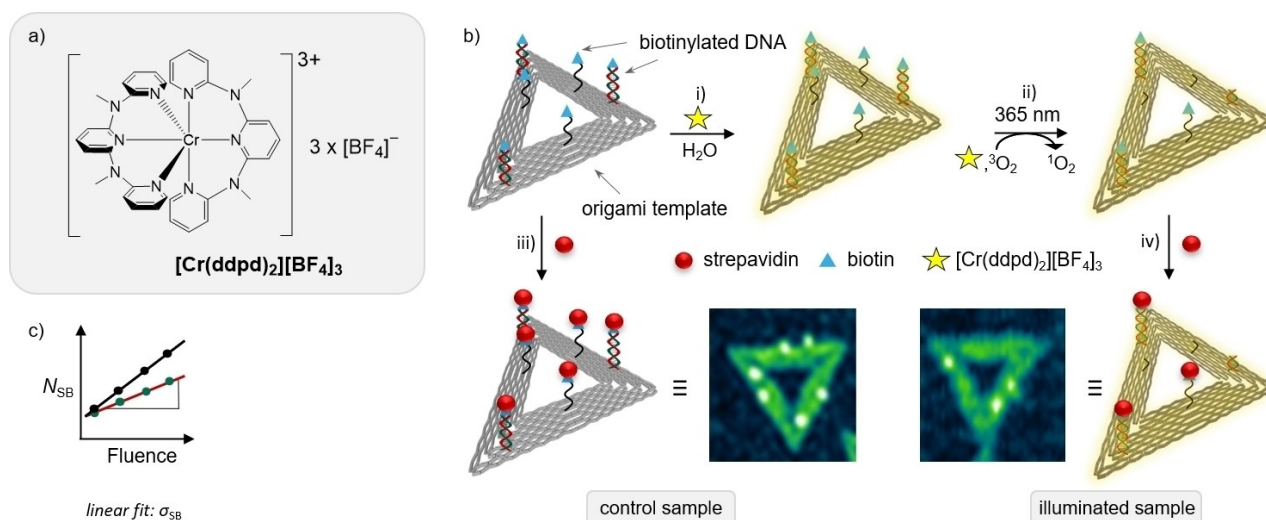
[c] Prof. Dr. K. Heinze
Department of Chemistry
Johannes Gutenberg University of Mainz
Duesbergweg 10–14, 55128 Mainz (Germany)

[d] Dr. C. Wang⁺
present address: Department of Chemistry
University of Basel
St. Johanns-Ring 19, 4056 Basel (Switzerland)

[⁺] These authors contributed equally to this manuscript.

 Supporting information for this article is available on the WWW under <https://doi.org/10.1002/chem.202203719>

 © 2023 The Authors. Chemistry - A European Journal published by Wiley-VCH GmbH. This is an open access article under the terms of the Creative Commons Attribution Non-Commercial License, which permits use, distribution and reproduction in any medium, provided the original work is properly cited and is not used for commercial purposes.



Scheme 1. a) Molecular structure of the water-soluble photosensitizer $[\text{Cr}(\text{ddpd})_2][\text{BF}_4]_3$; b) Scheme of the experimental procedure to absolutely determine the DNA strand break cross section σ_{SB} . Each DNA origami nanostructure (grey triangle) carries three biotinylated single (black wavy line) and double stranded (green-red wavy lines) DNA target sequences protruding from the template. (i) $[\text{Cr}(\text{ddpd})_2][\text{BF}_4]_3$ (yellow star) is added to the aqueous dispersion of DNA origamis covering the whole DNA origami template unspecifically. (ii) Generation of singlet oxygen $^1\text{O}_2$ upon UVA (365 nm) light illumination, and subsequent DNA strand breakage caused by $^1\text{O}_2$ and/or secondary ROS. After treating the non-illuminated (iii) and illuminated (iv) samples with streptavidin (red sphere), the intact DNA sequences are visualized with atomic force microscopy (AFM). Bright spots in the AFM images indicate streptavidin molecules attached to intact target sequences. c) Linear plots of the number of strand breaks N_{SB} as a function of the fluence yield slope values, corresponding to the strand break cross sections σ_{SB} .

states of the Cr^{III} sensitizer are quenched by oxygen via Dexter energy transfer with a rate constant k_q of $1.77 \times 10^7 \text{ M}^{-1} \cdot \text{s}^{-1}$ and a Stern-Volmer constant K_{SV} of $1.59 \times 10^4 \text{ M}^{-1}$,^[19a] yielding $^1\text{O}_2$.^[21a] First studies of the water-soluble $[\text{Cr}(\text{ddpd})_2][\text{BF}_4]_3$ complex as PS for PDT indicates no dark cytotoxicity, yet the highly positive charge of the complex prevents the efficient crossing of cell membranes.^[18e]

The oxidative stress caused by $^1\text{O}_2$ can result in DNA damage,^[24] affecting the physiological function of DNA and possibly leading to mutagenesis, carcinogenesis, aging or cell death. DNA damage by ROS has been explored by several groups using plasmid DNA^[25] and DNA oligonucleotides^[26] as model systems.^[12–14] An accurate and absolute quantification of DNA strand breaks is possible by the DNA origami technique,^[27] which can serve as a platform for single and double stranded DNA (ssDNA and dsDNA) target sequences. This technique allows to quantify radiation-induced single and double strand breaks in specific DNA sequences^[28] in terms of absolute cross sections σ_{SB} that can be directly compared to the photo-absorption cross sections σ_{PA} to determine quantum yields for strand breakage.^[29] This approach has been applied to study the strand cleavage in complex DNA structures with defined sequence,^[30] oligonucleotide length^[31] and topology^[32] induced by low-energy electrons,^[33] vacuum UV light,^[29] and gamma rays.^[34] However, the DNA origami technique was not yet utilized to quantify DNA strand breaks induced in the presence of ROS generated by a PS with UVA-Vis-NIR light illumination (310–800 nm, that is, 1.5–4.0 eV).

Efforts have been made to selectively generate $^1\text{O}_2$ in a spatially controlled manner for DNA damage.^[35] However, the quantitative assessment of DNA strand breaks mediated by $^1\text{O}_2$

and/or further ROS produced by a PS with low-energy radiation is very challenging and consequently rarely explored. Here, we explore the potential of the water-soluble luminescent molecular ruby $[\text{Cr}(\text{ddpd})_2][\text{BF}_4]_3$ (Scheme 1a) as a PS for selectively generating $^1\text{O}_2$ as initial reactive species under UVA-Vis light illumination. DNA strand breaks induced upon photoexcitation of this Cr^{III} complex are assessed on the single molecular level with the DNA origami technique, which allows to determine the quantum yield for strand breakage.

Results and Discussion

The highly positively charged Cr^{III} complex $[\text{Cr}(\text{ddpd})_2]^{3+}$ and the negatively charged DNA origamis are expected to electrostatically interact. Adding DNA origami to an aqueous $[\text{Cr}(\text{ddpd})_2]^{3+}$ (50 μM) solution under air leads to an increase of the absorption at 260 nm (Figure 1a, dotted lines), that is characteristic for the absorption of DNA origamis. Neither the absorption spectrum of the DNA origamis nor the Cr^{III} complex, however, change as confirmed by the difference of the absorption spectra of the individual components and the mixture of both species (Figure 1a; Supporting Information), Figure S1). This finding also indicates that the Cr^{III} complex does not intercalate into the DNA double helix, in contrast to observations with other Cr^{III} complexes, where the addition of DNA led to absorption changes of the employed PS due to their intercalation.^[18d,36] In addition, typically, different lifetimes are obtained when a chiral complex intercalates into the DNA double helix due to the different binding efficiencies of the enantiomers.^[37] In the presence of DNA origamis, the lumines-

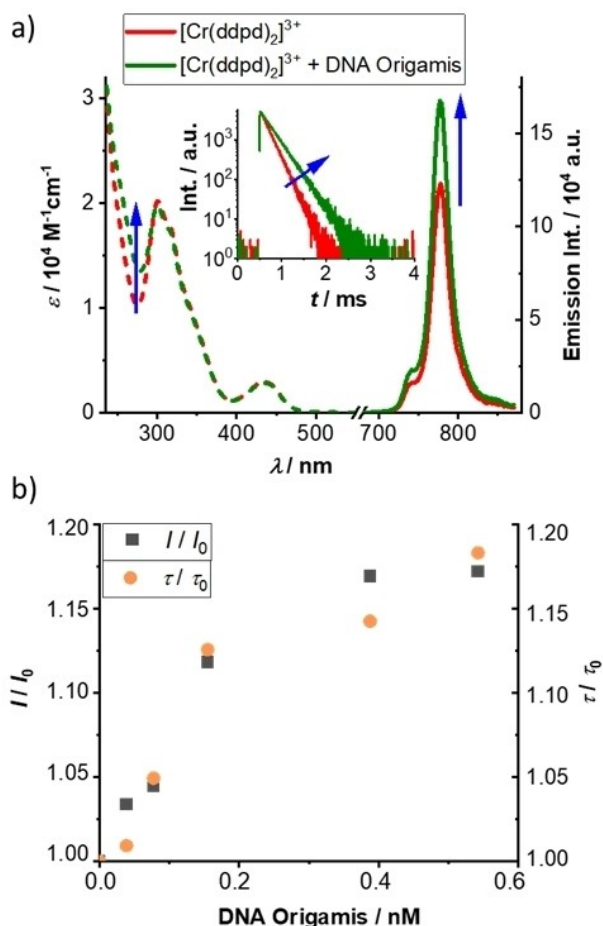


Figure 1. a) Absorption and luminescence spectra and luminescence decays of $[\text{Cr}(\text{ddpd})_2][\text{BF}_4]_3$ (50 μM) in air-saturated water in the absence (red) and presence (green) of DNA origamis (0.77 nM); b) Luminescence intensity ($I_{670-850}$) and lifetime (τ_{778}) of $[\text{Cr}(\text{ddpd})_2][\text{BF}_4]_3$ (20 μM) in air-saturated water as a function of increasing concentrations of DNA origamis (0–0.54 nM). Excitation was at 435 nm.

cence decay kinetics of the Cr^{III} complex, however, still show a mono-exponential behavior (Figure 1a, Figure S4b). This provides another hint that there is no distinct intercalation into the DNA. The presence of DNA origamis, however, increases the luminescence quantum yield and lifetime of the Cr^{III} complex under air from initially 2.1% and 180 μs to 3.0% and 270 μs , respectively (Figure 1a). The amplification in luminescence intensity and lifetime of the Cr^{III} complex (Figure 1b; Supporting Information, Figure S4) increases with increasing concentration of the DNA origamis up to a concentration of ~ 0.4 nM, and slowly approaches a saturation. This luminescence enhancement evidenced that a Type I mechanism (photo-induced electron transfer from DNA to the Cr^{III} complex) is not operative for the Cr^{III} complex and DNA. Other Cr^{III} complexes are photooxidants^[21b,38] and can oxidize DNA guanine bases via the Type I mechanism.^[18d,36,39] However, this is thermodynamically not feasible for $[\text{Cr}(\text{ddpd})_2]^{3+}$ due to its low excited state redox potential ($E_{1/2}([\text{Cr}(\text{ddpd})_2]^{3+}/[\text{Cr}(\text{ddpd})_2]^{2+}) = 0.49 \text{ V}$ vs. ferrocene).^[19a,21] Apparently, the electrostatic interactions be-

tween the positively charged Cr^{III} complex and the negatively charged DNA origamis lead either to a partial rigidification of the complex, hampering non-radiative relaxation pathways, and/or a slight shielding of the emissive Cr^{III} center from oxygen quenching. A similar luminescence enhancement of a Cr^{III} complex under aerated conditions was only recently observed by us in the presence of bulky counter anions^[40] and by employing sterically demanding ligands.^[41]

Apparent DNA binding makes the water-soluble Cr^{III} complex a suitable PS for DNA strand break studies with the DNA origami technique. Scheme 1b) highlights the DNA strand break determination and the experimental procedure to absolutely determine the DNA strand break cross sections (σ_{SB}) using DNA origami nanostructures as a platform for the investigation of arbitrary DNA target sequences. DNA origami templates (grey) are assembled from a long circular, ssDNA scaffold strand and a set of over 200 well-designed staple strands. Each staple strand can be addressed and individually functionalized with ssDNA (5'-d(GTG)₄, black curve) and dsDNA (5'-d(GTG)₄T₂(Bt-dT)(CAC)₄, red-green curve) target sequences protruding from the template. Route iii) shows the biotinylated (light blue triangle) target sequences reacted with streptavidin (red sphere) to visualize the intact DNA sequences with atomic force microscopy (AFM). The bright spots indicate streptavidin molecules attached to intact target sequences.

Adding water-soluble $[\text{Cr}(\text{ddpd})_2][\text{BF}_4]_3$ to the DNA origami nanostructures in route i) results in non-specific binding. Upon low-dose UVA light (365 nm) illumination (route ii), the Cr^{III} PS produces $^1\text{O}_2$ (Figure S2) close to the DNA target sequences, where DNA strand breaks were observed. In water, singlet oxygen has a lifetime of $\sim 3.5 \mu\text{s}$ and consequently a short diffusion path length of $\sim 220 \text{ nm}$, supporting interactions in a close proximity.^[42] On the other hand, the DNA origamis remain intact under these illumination conditions in the absence of the Cr^{III} PS (Figure S5).^[43] Treating the illuminated DNA origamis with streptavidin reveals a clear decrease in the number of intact DNA target sequences (route iv). Although $^1\text{O}_2$ normally cannot directly induce DNA strand breaks,^[44] yet strand breaks of plasmid DNA have been observed with a series of Ru^{II} and Os^{II} complexes with extended π -systems utilized as PS for generating $^1\text{O}_2$.^[45] Alternatively, the formed $^1\text{O}_2$ can react with aliphatic amines such as ethylenediaminetetraacetic acid (EDTA) present in the stock solution to give superoxide and ultimately hydroxyl radical, which can lead to DNA strand breaks.^[5b,21a,46]

AFM images of nanostructures treated with $[\text{Cr}(\text{ddpd})_2][\text{BF}_4]_3$ are displayed in Figure 2. The control sample (a), that was kept in the dark, and the sample illuminated with UVA light (365 nm) light (b) show well-shaped DNA origami triangles. $[\text{Cr}(\text{ddpd})_2][\text{BF}_4]_3$ treated DNA origami nanostructures show slight changes in the profile in the Ångström (10^{-10} m) range compared to a non-treated sample. The enlarged (zoomed-in) AFM images (centre) of a single DNA origami triangle before (top) and after (down) treatment with Cr^{III} and illumination show white spots at the central and side positions indicating streptavidin molecules bound to the intact DNA target sequences. The cross sections of DNA strand breaks σ_{SB} were absolutely determined by measuring the photon fluences of the

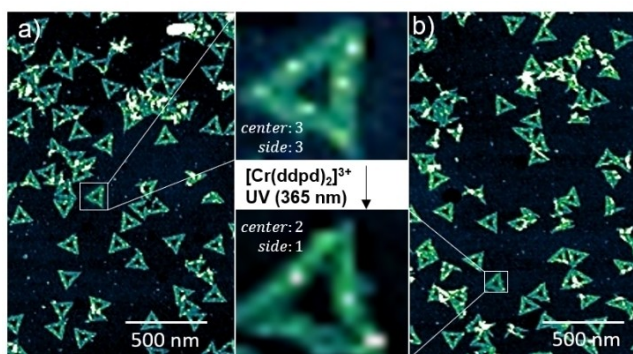


Figure 2. AFM images of a) a DNA origami control sample kept in the dark and b) a DNA origami sample mixed with $[\text{Cr}(\text{ddpd})_2][\text{BF}_4]_3$ and illuminated with UV light (365 nm, 0.60 mW cm^{-2}) for 120 seconds; The center shows enlarged AFM images of a single DNA origami template before (top) and after (down) treatment and illumination. The white spots on the central and side positions of the DNA origami nanostructures are streptavidin moieties bound to the intact DNA target sequences. The number of strand breaks N_{SB} can be determined by analyzing the two different sequences, that were illuminated and kept in the dark.

UVA light (365 nm) and detecting the DNA damages via AFM on a single molecule level. A detailed description of the determination of the photon fluences is given in the Experimental Section below. The linear fit of the number of strand breaks N_{SB} as a function of photon fluence gives σ_{SB} and represents a measure of the strand break probability (Scheme 1c).

Upon illumination with 365 nm UV light, no photodecomposition of the Cr^{III} complex is observed for at least 40 minutes (Figure S3), underlining its photostability.^[47] No DNA damage occurred for dsDNA and ssDNA under the same UVA light illumination conditions in the absence of the Cr^{III} PS (Figure 3a). Adding different concentrations (5, 20, and $50 \mu\text{M}$) of $[\text{Cr}(\text{ddpd})_2][\text{BF}_4]_3$ leads to a clear increase in N_{SB} as shown in the exposure-response curves (Figure 3 b–d); Supporting Information, Figure S6). Higher concentrations of the Cr^{III} PS yield higher σ_{SB} values, as observed for both ssDNA and dsDNA, resulting in a faster saturation of N_{SB} . The saturation is caused by interstrand crosslinkages on the DNA origami nanostructures, leaving cleaved DNA strands on the triangular origami surface.

A DSB requires two SSBs on opposite strands in close proximity (within a few DNA nucleotides). The linear dependence of DSBs on photon number indicates that a single photon is able to induce a DSB. A single photon first induces formation of one $^1\text{O}_2$ molecule, which then leads to strand breaks in two closely spaced strands. Although the details of this process remain to be elucidated, it is clear that the probability of a DSB is expected to be lower than that of a SSB. Nevertheless, for lower Cr^{III} complex concentrations ($< 20 \mu\text{M}$), the strand break cross section for dsDNA (σ_{DSB}) and ssDNA (σ_{SSB}) are similar, while in the presence of $50 \mu\text{M}$ Cr^{III} complex, the σ_{SSB} value is 1.6 times higher than the σ_{DSB} value. This observation suggests the preferential binding of the Cr^{III} complex to dsDNA resulting in a higher number of DSBs than SSBs as long as no saturation of occupation sites is reached. For a Cr^{III} complex concentration of

$50 \mu\text{M}$, the number of Cr^{III} complexes roughly equals the total number of nucleotides in the DNA origami sample. Therefore, all binding sites including ssDNA should be occupied by a Cr^{III} complex. As a result, σ_{SSB} significantly exceeds σ_{DSB} for high Cr^{III} concentrations.

The absolute determination of strand break cross sections allows to calculate the quantum yield of strand breakage, that is the number of photons absorbed by the Cr^{III} complex that are required for a DNA strand break (see Supporting Information, Table S2). Thereby, depending on the Cr^{III} complex concentration, we find quantum yield values ranging between 0.013 to 0.042. DSBs are the most severe form of DNA damage and the quantum yield for DSBs appears to reach a saturation around 0.027 (corresponding to 37 absorbed photons required to induce one DSB) indicating that at this concentration, all DNA binding sites for the Cr^{III} complex are occupied.

Conclusion and Outlook

In summary, the water-soluble molecular ruby $[\text{Cr}(\text{ddpd})_2][\text{BF}_4]_3$ was used as a photosensitizer (PS) to generate singlet oxygen ($^1\text{O}_2$) under low energy UVA light illumination at 365 nm and the resulting DNA strand breaks were quantified by the DNA origami technique and AFM. Electrostatic interactions between the positively charged Cr^{III} complex and the negatively charged DNA sequences favor the binding of the Cr^{III} PS to DNA, leading to efficient conversion of UVA photons into DNA strand breaks. The DNA strand break cross sections σ_{SB} were absolutely determined from the photon fluence and the DNA strand breaks at the single molecule level with AFM. The σ_{SB} obtained for both single and double stranded DNA showed a clear dependence on Cr^{III} complex concentration. For Cr^{III} complex concentrations below $50 \mu\text{M}$ and the chosen DNA origami concentration, not all possible binding sites are occupied with Cr^{III} complexes. At $50 \mu\text{M}$ Cr^{III} the quantum yield for DNA strand breakage reached maximum values of 0.042 and 0.027 for single strand breaks (SSBs) and double strand breaks (DSBs), respectively.

Overall, this study expands the toolbox of PS based on Cr^{III} complexes for the efficient generation of $^1\text{O}_2$, which can be used for controlled DNA damage. In addition, our DNA origami approach in conjunction with AFM readout offers a new method for the quantitative determination of DNA damage in aqueous solution with low energy photon illumination. In the future we aim to gain more mechanistic insight into the interactions between the Cr^{III} complex and DNA origamis as well as the mechanism of the DNA strand breaks. We also plan to expand these studies to other Cr^{III} complexes with long excited state lifetimes, that allow for $^1\text{O}_2$ formation.

Experimental Section

Materials: $[\text{Cr}(\text{ddpd})_2][\text{BF}_4]_3$ was prepared according to the literature.^[19,40]

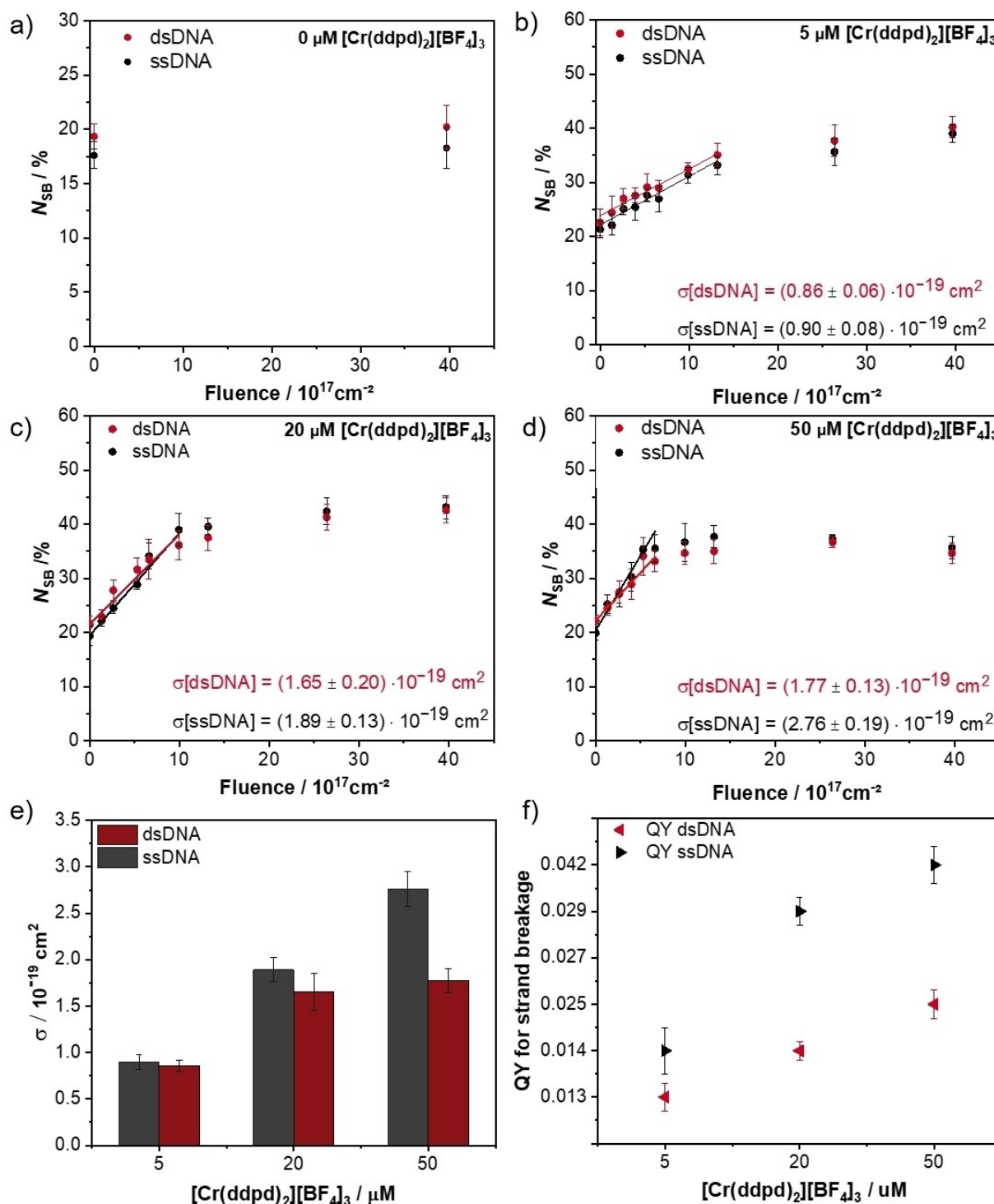


Figure 3. Number of strand breaks N_{SB} as a function of the illuminating photon fluence at 365 nm a) in the absence and b–d) in the presence of $[\text{Cr}(\text{ddpd})_2][\text{BF}_4]_3$ with concentrations of b) 5 μM, c) 20 μM, and d) 50 μM, respectively. e) Bar chart of the absolutely determined DNA strand break cross section σ_{SB} for ssDNA (black) and dsDNA (red) in dependence of the $[\text{Cr}(\text{ddpd})_2][\text{BF}_4]_3$ concentration. f) Quantum yield for strand breakage.

DNA origami triangles was prepared and modified according to the literature.^[48]

For one batch of DNA origami assembly, 5 μL of 100 nM viral scaffold strand M13mp18, 202 short ssDNA (3 μL each) are mixed with 10 μL of 10×TAE-buffer (Tris-acetate-EDTA with 125 mM MgCl_2), 6×1.5 μL of 100 nM modified target sequences, and 46 μL

deionized water. During an annealing process, the DNA nanostructures were heated up to 80 °C and stepwise cooled down over 2 h to 6 °C. The solution of self-assembled triangular-shaped DNA origami is filtered three times with 1×TAE-buffer containing 12.5 mM MgCl_2 for 6 min at 4629 g. Each DNA origami substrate carries two different biotinylated target sequences at fixed

positions (dsDNA HP-1 = (GTG)₄T(Bt-dT)₂(CAC)₄) / ssDNA (GTG)₄-Bt). For the illumination experiments several batches of DNA origami structures were pooled to yield a solution of 31 nM DNA origami triangles in 0.5 mL of water (containing 1×TAE-buffer and 12.5 mM MgCl₂). For the illumination experiments, 125 μL of 31 nM DNA origami was mixed with the Cr^{III} complex in milli-Q water to arrive at a 1 mL aqueous solution with the indicated Cr^{III} complex concentration.

Irradiation was performed in aqueous solution at 365 nm with the indicated time, up to one hour. The irradiated DNA nanostructures are immobilized on 8×8 mm² air plasma cleaned silicon substrates by mixing 2 μL of irradiated solution with 15 μL of 10×TAE-buffer with 125 mM MgCl₂ and incubation on Si for 1 h. After that 15 μL 50 nM SAV was added for 2 min and subsequently rinsed with 500 μL of 1:1 deionized water/ethanol.

UV/Vis absorption spectra were recorded with the Varian Cary 5000 spectrometer using 1.0 cm quartz cells.

Luminescence measurements: Luminescence emission spectra and luminescence decays of the [Cr(dddpd)₂][BF₄]₃ in the absence and presence of DNA origamis were obtained with a calibrated spectrofluorometer FSP 920 from Edinburgh Instruments. For the measurement of the emission spectra, a CW xenon lamp was used as the excitation light source, while the time-resolved luminescence measurements were performed with a μs xenon flashlamp (100 Hz) and single photon counting detection in a multi-channel scaling mode.

AFM measurements: Irradiated samples are incubated with 50 nM streptavidin (SAV) solution. Damaged DNA oligonucleotides on the DNA origami triangles can be visualized with atomic force microscopy (Agilent 5500) operated in tapping mode using a cantilever Tap 150 Al-G with a resonance frequency of 150 kHz and a spring constant of 5 N/m. The SAV is detected by a bright spot on the DNA origami indicating an intact DNA oligonucleotide with no strand break. The binding efficiency of streptavidin to biotin is not 100%, and it is also possible that not every oligonucleotide actually bears a biotin (due to the limited coupling efficiency during the synthesis or other processes during the handling of the DNA samples). This leads to a basic non-zero level of “observed strand breaks”, however, this level is constant within one set of illumination experiments. This demonstrates that one whole series of illumination experiments must be performed under identical conditions using the same batch of samples. On each sample four images are recorded with a size of 4×4 μm² and a resolution of 1024 pixels/line. Depending on the density of the immobilized DNA nanostructures, each AFM image usually contains 1000–2000 DNA origami triangles.

Measurements of photon numbers: The photon number was calculated by using the determined UVA light (365 nm, Advantage-Lab™ UV Lamp, 2×15 Watt, Fischer Scientific) power density divided by the energy of one photon. This quantity was measured with a power meter (Newport 841-PE power meter) placed at sample position with a detector area of 1 cm² and a customized calibrated sphere setup with a detector area of 3.14 cm², respectively. Power density values measured with both setups were determined to be 0.60 mW/cm² with a derivation within 10%. Dividing the energy of one photon of 365 nm, the photon number per area per second was calculated to be 1.1×10¹⁵ s⁻¹cm⁻². According to the different illumination times, the photon numbers per area are calculated (Supporting Information, Table S1).

Acknowledgements

This work was supported by the Deutsche Forschungsgemeinschaft (RE 1203/23-2, HE 2778/10-2) and the European Research Council (ERC Consolidator Grant 772752). Open Access funding enabled and organized by Projekt DEAL.

Conflict of Interest

The authors declare no conflict of interest.

Data Availability Statement

The data that support the findings of this study are available from the corresponding author upon reasonable request.

Keywords: chromium · DNA origami · DNA strand breaks · photodynamic therapy · photosensitizer

- [1] G. Gunaydin, M. E. Gedik, S. Ayan, *Front. Chem.* **2021**, *9*, 686303.
- [2] a) M. C. DeRosa, R. J. Crutchley, *Coord. Chem. Rev.* **2002**, *233–234*, 351–371; b) G. Gunaydin, M. E. Gedik, S. Ayan, *Front. Chem.* **2021**, *9*, 691697.
- [3] J. Moan, K. Berg, *Photochem. Photobiol.* **1991**, *53*, 549–553.
- [4] F. Heinemann, J. Karges, G. Gasser, *Acc. Chem. Res.* **2017**, *50*, 2727–2736.
- [5] a) A. P. Castano, P. Mroz, M. R. Hamblin, *Nat. Rev. Cancer* **2006**, *6*, 535–545; b) I. Nakanishi, S. Fukuzumi, T. Konishi, K. Ohkubo, M. Fujitsuka, O. Ito, N. Miyata, *J. Phys. Chem. B* **2002**, *106*, 2372–2380.
- [6] H. Abrahamse, M. R. Hamblin, *Biochem. J.* **2016**, *473*, 347–364.
- [7] a) M. Lan, S. Zhao, W. Liu, C. S. Lee, W. Zhang, P. Wang, *Adv. Healthcare Mater.* **2019**, *8*, 1900132; b) M. Liu, C. Li, *ChemPlusChem* **2020**, *85*, 948–957.
- [8] A. B. Ormond, H. S. Freeman, *Materials* **2013**, *6*, 817–840.
- [9] a) R. Bonnett, *Chem. Soc. Rev.* **1995**, *24*, 19–33; b) P. C. Lo, M. S. Rodriguez-Morgade, R. K. Pandey, D. K. P. Ng, T. Torres, F. Dumoulin, *Chem. Soc. Rev.* **2020**, *49*, 1041–1056.
- [10] a) K. Urbanska, B. Romanowska-Dixon, Z. Matuszak, J. Oszejka, P. Nowak-Sliwinska, G. Stochel, *Acta Biochim. Pol.* **2002**, *49*, 387–391; b) C. Shirata, J. Kaneko, Y. Inagaki, T. Kokudo, M. Sato, S. Kiritani, N. Akamatsu, J. Arita, Y. Sakamoto, K. Hasegawa, N. Kokudo, *Sci. Rep.* **2017**, *7*, 13958.
- [11] a) S. Radunz, S. Wedepohl, M. Rohr, M. Calderon, H. R. Tschiche, U. Resch-Genger, *J. Med. Chem.* **2020**, *63*, 1699–1708; b) A. Turksoy, D. Yildiz, E. U. Akkaya, *Coord. Chem. Rev.* **2019**, *379*, 47–64.
- [12] a) W. Fudickar, M. Bauch, H. Ihmels, T. Linker, *Chem. Eur. J.* **2021**, *27*, 13591–13604; b) W. Fudickar, P. Roder, M. Listek, K. Hanack, T. Linker, *Photochem. Photobiol.* **2022**, *98*, 193–201.
- [13] a) H. He, X. Zheng, S. Liu, M. Zheng, Z. Xie, Y. Wang, M. Yu, X. Shuai, *Nanoscale* **2018**, *10*, 10991–10998; b) Y. Cai, P. Liang, Q. Tang, W. Si, P. Chen, Q. Zhang, X. Dong, *ACS Appl. Mater. Interfaces* **2017**, *9*, 30398–30405.
- [14] a) S. Liu, G. Feng, B. Z. Tang, B. Liu, *Chem. Sci.* **2021**, *12*, 6488–6506; b) G. Yi, S. H. Hong, J. Son, J. Yoo, C. Park, Y. Choi, H. Koo, *Quant. Imaging Med. Surg.* **2018**, *8*, 433–443.
- [15] a) S. Monro, K. L. Colon, H. Yin, J. Roque, 3rd, P. Konda, S. Gujar, R. P. Thummel, L. Lilge, C. G. Cameron, S. A. McFarland, *Chem. Rev.* **2019**, *119*, 797–828; b) J. Zhao, W. Wu, J. Sun, S. Guo, *Chem. Soc. Rev.* **2013**, *42*, 5323–5351; c) K. Mitra, S. Gautam, P. Kondaiah, A. R. Chakravarty, *Angew. Chem. Int. Ed.* **2015**, *54*, 13989–13993; *Angew. Chem.* **2015**, *127*, 14195–14199; d) U. Basu, I. Khan, A. Hussain, P. Kondaiah, A. R. Chakravarty, *Angew. Chem. Int. Ed.* **2012**, *51*, 2658–2661; *Angew. Chem.* **2012**, *124*, 2712–2715; e) M. A. Sgambellone, A. David, R. N. Garner, K. R. Dunbar, C. Turro, *J. Am. Chem. Soc.* **2013**, *135*, 11274–11282; f) H. Huang, B. Yu, P. Zhang, J. Huang, Y. Chen, G. Gasser, L. Ji, H. Chao, *Angew. Chem. Int. Ed.* **2015**, *54*, 14049–14052; *Angew. Chem.* **2015**, *127*, 14255–14258; g) S. Banerjee, A. R. Chakravarty, *Acc. Chem. Res.* **2015**, *48*, 2075–

- 2083; h) C. Imberti, P. Zhang, H. Huang, P. J. Sadler, *Angew. Chem. Int. Ed.* **2020**, *59*, 61–73; *Angew. Chem.* **2020**, *132*, 61–73.
- [16] a) J. Soriano, A. Villanueva, J. C. Stockert, M. Canete, *Histochem. Cell Biol.* **2013**, *139*, 149–160; b) H. Abrahamse, M. R. Hamblin, *Biochem. J.* **2016**, *473*, 347–364; c) T. Sarkar, A. Kumar, S. Sahoo, A. Hussain, *Inorg. Chem.* **2021**, *60*, 6649–6662; d) J. Karges, U. Basu, O. Blacque, H. Chao, G. Gasser, *Angew. Chem. Int. Ed.* **2019**, *58*, 14334–14340; *Angew. Chem.* **2019**, *131*, 14472–14478; e) S. M. Pradeepa, H. S. Bhojya Naik, B. Vinay Kumar, K. Indira Priyadarsini, A. Barik, S. Jayakumar, *Inorg. Chim. Acta* **2015**, *428*, 138–146.
- [17] Y. Zhang, J. Zheng, Y. Jiang, X. Huang, L. Fang, *Front. Pharmacol.* **2020**, *11*, 1166.
- [18] a) J. Toneatto, P. F. Garcia, G. A. Arguello, *J. Inorg. Biochem.* **2011**, *105*, 1299–1305; b) P. F. Garcia, J. Toneatto, M. J. Silvero, G. A. Arguello, *Biochim. Biophys. Acta* **2014**, *1840*, 2695–2701; c) J. Toneatto, G. A. Arguello, *J. Inorg. Biochem.* **2011**, *105*, 645–651; d) F. A. Baptista, D. Krizan, M. Stitch, I. V. Sazanovich, I. P. Clark, M. Towrie, C. Long, L. Martinez-Fernandez, R. Improta, N. A. P. Kane-Maguire, J. M. Kelly, S. J. Quinn, *J. Am. Chem. Soc.* **2021**, *143*, 14766–14779; e) U. Basu, S. Otto, K. Heinze, G. Gasser, *Eur. J. Inorg. Chem.* **2019**, 37–41.
- [19] a) S. Otto, M. Grabolle, C. Förster, C. Kreitner, U. Resch-Genger, K. Heinze, *Angew. Chem. Int. Ed.* **2015**, *54*, 11572–11576; *Angew. Chem.* **2015**, *127*, 11735–11739; b) C. Wang, S. Otto, M. Dorn, E. Kreidt, J. Lebon, L. Srsan, P. Di Martino-Fumo, M. Gerhards, U. Resch-Genger, M. Seitz, K. Heinze, *Angew. Chem. Int. Ed.* **2018**, *57*, 1112–1116; *Angew. Chem.* **2018**, *130*, 1125–1130.
- [20] a) S. Otto, N. Scholz, T. Behnke, U. Resch-Genger, K. Heinze, *Chem. Eur. J.* **2017**, *23*, 12131–12135; b) S. Otto, J. P. Harris, K. Heinze, C. Reber, *Angew. Chem. Int. Ed.* **2018**, *57*, 11069–11073; *Angew. Chem.* **2018**, *130*, 11236–11240; c) C. Wang, S. Otto, M. Dorn, K. Heinze, U. Resch-Genger, *Anal. Chem.* **2019**, *91*, 2337–2344.
- [21] a) S. Otto, A. M. Nauth, E. Ermilov, N. Scholz, A. Friedrich, U. Resch-Genger, S. Lochbrunner, T. Opatz, K. Heinze, *ChemPhotoChem* **2017**, *1*, 344–349; b) S. Sittel, R. Naumann, K. Heinze, *Front. Chem.* **2022**, *10*, 887439.
- [22] a) J. Kalmbach, C. Wang, Y. You, C. Förster, H. Schubert, K. Heinze, U. Resch-Genger, M. Seitz, *Angew. Chem. Int. Ed.* **2020**, *59*, 18804–18808, *Angew. Chem.* **2020**, *132*, 18966–18970; b) C. Wang, F. Reichenauer, W. R. Kitzmann, C. Kerzig, K. Heinze, U. Resch-Genger, *Angew. Chem. Int. Ed.* **2022**, *61*, e202202238; *Angew. Chem.* **2022**, *134*, e202202238.
- [23] C. Dee, F. Zinna, W. R. Kitzmann, G. Pescitelli, K. Heinze, L. Di Bari, M. Seitz, *Chem. Commun.* **2019**, *55*, 13078–13081.
- [24] S. Shahmoradi Ghahe, K. Kosicki, M. Wojewodzka, B. A. Majchrzak, A. Fogtman, R. Iwanicka-Nowicka, A. Ciuba, M. Koblowska, M. Kruszewski, B. Tudek, E. Speina, *DNA Repair* **2021**, *104*, 103136.
- [25] C. M. Berra, C. F. M. Menck, G. R. Martinez, C. S. de Oliveira, M. d. S. Baptista, P. D. Mascio, *Quim. Nova* **2010**, *33*, 279–283.
- [26] C. Bohne, K. Faulhaber, B. Giese, A. Häfner, A. Hofmann, H. Ihmels, A.-K. Köhler, S. Perä, F. Schneider, M. A. L. Sheepwash, *J. Am. Chem. Soc.* **2005**, *127*, 76–85.
- [27] A. Keller, I. Bald, A. Rotaru, E. Cauët, K. V. Gothelf, F. Besenbacher, *ACS Nano* **2012**, *6*, 4392–4399.
- [28] a) K. Ebel, I. Bald, *J. Phys. Chem. Lett.* **2022**, *13*, 4871–4876; b) R. Schurmann, S. Vogel, K. Ebel, I. Bald, *Chem. Eur. J.* **2018**, *24*, 10271–10279.
- [29] S. Vogel, J. Rackwitz, R. Schürman, J. Prinz, A. R. Milosavljević, M. Réfrégiers, A. Giuliani, I. Bald, *J. Phys. Chem. Lett.* **2015**, *6*, 4589–4593.
- [30] S. Vogel, K. Ebel, R. M. Schurmann, C. Heck, T. Meiling, A. R. Milosavljević, A. Giuliani, I. Bald, *ChemPhysChem* **2019**, *20*, 823–830.
- [31] K. Ebel, I. Bald, *Int. J. Mol. Sci.* **2020**, *21*, 111.
- [32] J. Rackwitz, I. Bald, *Chemistry* **2018**, *24*, 4680–4688.
- [33] R. Schurmann, T. Tsering, K. Tanzer, S. Denifl, S. V. K. Kumar, I. Bald, *Angew. Chem. Int. Ed.* **2017**, *56*, 10952–10955; *Angew. Chem.* **2017**, *129*, 11094–11098.
- [34] L. Sala, A. Zerolova, A. Rodriguez, D. Reimitz, M. Davidkova, K. Ebel, I. Bald, J. Kocisek, *Nanoscale* **2021**, *13*, 11197–11203.
- [35] T. Tørring, S. Helmig, P. R. Ogilby, K. V. Gothelf, *Acc. Chem. Res.* **2014**, *47*, 1799–1806.
- [36] V. G. Vaidyanathan, B. U. Nair, *Eur. J. Inorg. Chem.* **2004**, 1840–1846.
- [37] R. Vijayalakshmi, M. Kanthimathi, R. Parthasarathi, B. U. Nair, *Bioorg. Med. Chem.* **2006**, *14*, 3300–3306.
- [38] a) N. Serpone, M. A. Jamieson, M. S. Henry, M. Z. Hoffman, F. Bolletta, M. Maestri, *J. Am. Chem. Soc.* **1979**, *101*, 2907–2916; b) R. Ballardini, G. Varani, F. Scandola, V. Balzani, *J. Am. Chem. Soc.* **1976**, *98*, 7432–7433; c) T. H. Burgin, F. Glaser, O. S. Wenger, *J. Am. Chem. Soc.* **2022**, *144*, 14181–14194; d) S. M. Stevenson, M. P. Shores, E. M. Ferreira, *Angew. Chem. Int. Ed.* **2015**, *54*, 6506–6510; *Angew. Chem.* **2015**, *127*, 6606–6610; e) S. Sittel, A. C. Sell, K. Hofman, C. Wiedemann, J. P. Nau, C. Kerzig, G. Manolikakes, K. Heinze, *ChemCatChem* **2023**, doi.org/10.1002/cctc.202201562.
- [39] R. T. Watson, N. Desai, J. Wildsmith, J. F. Wheeler, N. A. P. Kane-Maguire, *Inorg. Chem.* **1999**, *38*, 2683–2687.
- [40] C. Wang, W. R. Kitzmann, F. Weigert, C. Förster, X. Wang, K. Heinze, U. Resch-Genger, *ChemPhotoChem* **2022**, *6*, e202100296.
- [41] L. Stein, C. Wang, C. Förster, U. Resch-Genger, K. Heinze, *Dalton Trans.* **2022**, *51*, 17664–17670.
- [42] a) M. Bregnhøj, M. Westberg, F. Jensen, P. R. Ogilby, *Phys. Chem. Chem. Phys.* **2016**, *18*, 22946–22961; b) R. W. Redmond, I. E. Kochevar, *Photochem. Photobiol.* **2006**, *82*, 1178–1186.
- [43] W. Fang, M. Xie, X. Hou, X. Liu, X. Zuo, J. Chao, L. Wang, C. Fan, H. Liu, L. Wang, *J. Am. Chem. Soc.* **2020**, *142*, 8782–8789.
- [44] J. Cadet, S. Mouret, J. L. Ravanat, T. Douki, *Photochem. Photobiol.* **2012**, *88*, 1048–1065; b) P. Di Mascio, G. R. Martinez, S. Miyamoto, G. E. Ronsein, M. H. G. Medeiros, J. Cadet, *Chem. Rev.* **2019**, *119*, 2043–2086.
- [45] a) C. Mari, V. Pierroz, R. Rubbiani, M. Patra, J. Hess, B. Spingler, L. Oehninger, J. Schur, I. Ott, L. Salassa, S. Ferrari, G. Gasser, *Chem. Eur. J.* **2014**, *20*, 14421–14436; b) J. Hess, H. Huang, A. Kaiser, V. Pierroz, O. Blacque, H. Chao, G. Gasser, *Chem. Eur. J.* **2017**, *23*, 9888–9896; c) H. Huang, P. Zhang, B. Yu, C. Jin, L. Ji, H. Chao, *Dalton Trans.* **2015**, *44*, 17335–17345; d) Y. Sun, L. E. Joyce, N. M. Dickson, C. Turro, *Chem. Commun.* **2010**, *46*, 6759–6761.
- [46] a) D. P. Hessler, F. H. Frimmel, E. Oliveros, A. M. Braun, *Helv. Chim. Acta* **1994**, *77*, 859–868; b) Isao Saito, Teruo Matsuura, K. Inoue, *J. Am. Chem. Soc.* **1981**, *103*, 188–190.
- [47] S. Otto, M. Dorn, C. Förster, M. Bauer, M. Seitz, K. Heinze, *Coord. Chem. Rev.* **2018**, *359*, 102–111.
- [48] a) J. Rackwitz, M. L. Ranković, A. R. Milosavljević, I. Bald, *Eur. Phys. J. D* **2017**, *71*, 32; b) P. W. Rothmund, *Nature* **2006**, *440*, 297–302.

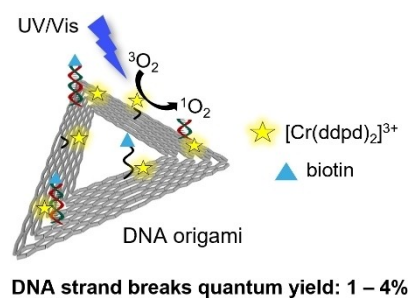
Manuscript received: November 29, 2022

Accepted manuscript online: February 3, 2023

Version of record online: ■■■

RESEARCH ARTICLE

Singlet oxygen sensitized by the molecular ruby $[\text{Cr}(\text{ddpd})_2]^{3+}$ under excitation with UV/Vis light induces DNA strand breaks. Utilization of the DNA origami technology together with atomic force microscopy enabled the quantification of the quantum yield of strand breaks to 1–4%, revealing the promising potential of using $[\text{Cr}(\text{ddpd})_2]^{3+}$ as photosensitizer for photodynamic therapy.



Dr. C. Wang, Dr. K. Ebel, Prof. Dr. K. Heinze, Dr. U. Resch-Genger, Prof. Dr. I. Bald**

1 – 8

Quantum Yield of DNA Strand Breaks under Photoexcitation of a Molecular Ruby

